$$= 2\pi (ff^2 - ff^2 \cot \kappa - g'^2 f\kappa + fg'^2 - r_1 f^2)$$

which in terms of ψ_b and θ gives

$$V_b = 2\pi r_1^3 [(1 - \cos\psi_b)\{\sin\psi_b + (1 - \cos\psi_b)\cot(\psi_b + \theta)\}^2 - (1 - \cos\psi_b{}^2)\{\sin\psi_b + (1 + \cos\psi_b)\cot(\psi_b + \theta)\}\cot(\pi/2 - \psi_b - \theta) - \left\{\frac{1 - \cos\psi_b}{\cos(\psi_b + \theta)}\right\}^2 [\sin\psi_b + (1 - \cos\psi_b)\cot(\psi_b + \theta)]\left(\frac{\pi}{2} - \psi_b - \theta\right) + (1 + \cos\psi_b)\left\{\frac{1 - \cos\psi_b}{\cos(\psi_b + \theta)}\right\}^2 - (1 - \cos\psi_b)^2] \quad (A8)$$

that is

$$V_b = 2\pi r_1^3 F_2(\psi_b, \theta)$$

The area of the 12 interface is that of a segment of a sphere and is given by

$$A_{12} = 2\pi r_1 f = 2\pi r_1^2 (1 - \cos\psi_b) \quad (A9)$$

and

$$A_{13} = 4\pi r_1^2 - 2\pi r_1 f = 2\pi r_1^2 (1 + \cos\psi_b) \quad (A10)$$

These expressions for A_b, A_{12}, and A_{13} can be substituted into Equation (10) to determine the free energy of state IV.

LITERATURE CITED

Albertsson, P. A., *Partition of Cell Particles and Macromolecules*, 2 ed., Wiley-Interscience, New York (1971).

Capes, C. E., "Basic Research in Particle Technology and Some Novel Applications," *Can. J. Chem. Eng.*, **54**, 3 (1976).

Doscher, T. M., "Tertiary Oil Recovery," *Chem. Tech.*, **7**, 232 (1977).

Erle, M. A., D. C. Dyson, and N. R. Morrown, "Liquid Bridges Between Cylinders, in a Torus, and Between Spheres," *AIChE J.*, **17**, 115 (1971).

Henry, J. D., M. E. Prudich, and A. D. Hovarongkura, "Ash Removal from Coal Derived Liquids by Extraction into an Aqueous Phase: Preliminary Feasibility Studies," Final report to ERDA, Grant #90155045, Dept. of Chemical Engineering, West Virginia Univ., Morgantown (1976).

Hotta, K., K. Takeda, and K. Iinoya, "The Capillary Binding Force of a Liquid Bridge," *Powder Tech.*, **10**, 231 (1974).

Mayer, R. P., and R. A. Stowe, "Mercury Porosimetry: Filling of Toroidal Void Volume Following Break through between Packed Spheres," *J. Phys. Chem.*, **70**, 3867 (1966).

Melrose, J. C., and G. C. Wallick, "Exact Geometrical Parameters for Pendular Ring Fluid," *ibid.*, **71**, 3676 (1967).

Melrose, J. C., "Model Calculations for Capillary Condensation," *AIChE J.*, **12**, 986 (1966).

Mizrahi, J., and E. Barnea, "The Effects of Solid Additives on the Formation and Separation of Emulsions," *Brit. Chem. Eng.*, **15**, 497 (1970).

———, "Systems Consisting of Two Liquid Phases and Solid Particles," *Progr. Heat Mass Trans.*, **6**, 717 (1972).

Moody, G. B., ed., *Petroleum Exploration Handbook*, McGraw-Hill, New York (1961).

Princen, H. M., "The Equilibrium Shape of Interfaces, Drops and Bubbles. Rigid and Deformable Particles at Interfaces," *Surface Colloid Sci.*, **2**, 1 (1969).

Prudich, M. E., and J. D. Henry, Jr., "The Mechanisms of Transfer of Hydrophobic Coated Matter Particles from a Hydrocarbon to an Aqueous Phase," *AIChE J.*, in press (1978).

Puddington, I. E., and B. D. Sparks, "Spherical Agglomeration Processes," *Min. Sci. Eng.*, **7**, 282 (1975).

Rapacchietta, A. V., and A. W. Neumann, "Force and Free-Energy Analyses of Small Particles at Fluid Interfaces. II. Spheres," *J. Colloid Interface Sci.*, **59**, 555 (1977).

Manuscript received October 3, 1977; revision received August 11, and accepted August 25, 1978.

An Analytical Study of Ultrafiltration in a Hollow Fiber Artificial Kidney

A theoretical investigation of ultrafiltration through hollow fibers used in artificial kidney applications is presented. The hollow fibers are considered to be cylindrical tubes with ideally selective semipermeable walls which retain cellular particles (red and white cells, platelets) and plasma proteins in the blood perfusing the fibers. In contrast, water and species of low and medium molecular weight can freely permeate the membranes. The assumption is made that secondary flows avoid the formation of concentration boundary layers at the wall. Proper nondimensionalization of the equations for axial and radial transport results in the identification of parameters which are important in the characterization of the ultrafiltration through semipermeable tubes. Perturbation analyses for small values of these parameters lead to sets of differential equations which were solved analytically. These closed form solutions demonstrate the influence of hydraulic conductivity of the fiber walls, geometry, and axial and transmembrane pressure drop on the efficiency of hollow fiber artificial kidneys.

HEINZ D. PAPENFUSS

JOSEPH F. GROSS

and

STEVEN T. THORSON

Department of Chemical Engineering
University of Arizona
Tucson, Arizona 85721

SCOPE

The purpose of an artificial kidney is to replace the function of the human kidney in the case of severe or complete renal failure. This function is to remove certain toxins of low and moderate molecular weight from the blood such as sodium chloride, potassium chloride, urea, creatinine, and uric acid. On the other hand, cellular particles and plasma proteins (macromolecules) should be retained in the blood lumen. Currently, most artificial

kidneys use species diffusion across a membrane as the mechanism to purify blood. This diffusive mass transport is referred to as dialysis or hemodialysis. A description of various artificial kidney devices based on this principle together with an analysis of the mass transfer mechanism is given by Cooney (1976).

Recently, a new design for an artificial kidney has received great attention in this country and abroad and is documented in the proceedings of the Tenth Annual Contractors Conference of the Artificial Kidney Program of the National Institute of Arthritis, Metabolism, and Digestive Diseases (1977). The driving force in this new artificial kidney is the pressure drop across a permselective membrane which controls the movement of water containing the small and medium molecular weight species mentioned above. However, the plasma proteins remaining in the blood build up a colloid osmotic pressure which acts against the hydrostatic pressure drop and thereby reduces the driving force for transmembrane water flow. In order to distinguish this type of blood purification from dialysis, the terms diafiltration, hemofiltration or hemodiafiltration are now used in the literature.

An important feature in diafiltration compared with dialysis is that the waste concentration is not changed during the filtration. Instead, this design calls for a reduction in the plasma volume which must be restored in a second stage by a fluid dilutant. Here the reduction of the waste concentration in the blood occurs. However, the present work is not concerned with processes which occur in the second stage.

The essential part of the artificial kidney which uses (ultra)filtration consists of a bundle of approximately 10 000 hollow fibers which are perfused with blood (Figure 1). The fiber walls are semipermeable membranes. The internal diameter of the fibers is about 200 μm; a typical fiber length is 17 cm. The transmembrane pressure can easily be adjusted in order to control the ultrafiltration rate. The advantages of these hemodiafilters compared with dialyzers are their small size and consequently small priming volume, low pressure drop, and low hemolysis rates (destruction of red blood cells) resulting from low shear rates.

Several factors limit the ultrafiltration efficiency of hollow fiber systems:

1. Concentration polarization, which is a formation of a concentration boundary layer near the membrane with a concomitant local increase in colloid osmotic pressure (Gill et al., 1971).

2. Reduced effective membrane hydraulic conductivity due to clogged pores caused by plasma proteins.

3. Gel formation at the membrane when the saturation concentration of the proteins is reached.

4. Increase in colloid osmotic pressure along the fiber axis due to fluid loss.

Gill and Bansal (1973) showed that the effect of concentration polarization can be neglected in hollow fiber, reverse osmosis systems if the wall Peclet number is less than 0.1. The wall Peclet number is defined as the ratio between transmembrane flux of solvent and diffusive flux of species in the solution normal to the membrane.

The wall Peclet number in blood ultrafiltration is usually greater than 100. This should lead to the conclusion that the effect of concentration polarization can generally not be neglected. However, an analytical or numerical treatment of this problem would be extremely complicated owing to the strong concentration gradients appearing near the wall. This is a singular perturbation problem of the boundary layer type which can be treated by the method of matched asymptotic expansions as has been done by Papenfuss et al. (1978) for ultrafiltration of aqueous solutions using flat membranes. In the case of ultrafiltration of blood, however, it can be expected that the presence of cellular particles leads to a certain degree of radial mixing which prevents the buildup of a concentration-boundary layer. This is especially so because those cellular particles that float near the wall tend to move inward to the center, thus producing both a cell poor plasma layer and a secondary flow (Charm and Kurland, 1974).

Additional secondary flows can be induced, for example, by rotation of the entire ultrafiltration unit which could support radial mixing. In the present work, we assume that the plasma proteins are well mixed in the radial direction and, therefore, do not consider the effects mentioned in 2 and 3.

The purpose of this analysis is to study the effects of geometry, membrane characteristics, and flow conditions on the ultrafiltration in hollow fiber systems using the idealized model mentioned above. Since hemodiafiltration resembles the process of blood purification which takes place in the human kidney, we have utilized earlier theoretical studies on renal blood flow. The basic ideas of our theoretical model follow the approach proposed by Huss et al. (1975) for renal filtration. Our analysis and results should be useful in the initiation of new experiments using single hollow fibers, and they should provide the framework for optimum design studies of hollow fiber artificial kidneys. The dimensionless treatment of the transport equations makes it possible to extend our results to hollow fiber reverse osmosis systems for use in desalination.

CONCLUSIONS AND SIGNIFICANCE

A theoretical study of ultrafiltration through hollow fibers used in artificial kidney machines is presented. The equations which govern this problem are those describing the conservation of mass and momentum in the laminar flow of blood through cylindrical tubes with semipermeable walls. The walls are assumed to be ideally selective membranes which prevent the penetration of cellular particles and plasma proteins while permitting water and salts to permeate freely. Therefore, hollow fiber ultrafiltration does not change the salt concentration in the blood. Instead, it reduces the plasma volume which is subsequently restored in a second stage with a diluting fluid. This leads to a consequent reduction in the salt concentration. The flow through the tubular walls is determined using a relationship which has been derived by Katchalsky (1965) on the basis of nonequilibrium thermodynamics. This equation reflects the fact that the effective ultrafiltration pressure is the hydrostatic pressure difference across the wall minus the colloid osmotic pressure established by the plasma proteins. During filtration, the plasma protein concentration increases which consequently causes an increase in the osmotic pressure, thus limiting the filtration rate. Additional effects which limit ultrafiltration through semipermeable membranes are concentration polarization at the wall, reduced effective membrane conductivity due to clogged pores, and gel formation at the wall, when the saturation concentration of the proteins is reached. These additional effects are not considered in the present work.

This analysis leads to a coupled set of nonlinear differential equations for axial and radial transport. Nondimensionalization of these equations results in identification of

parameters which play key roles in characterizing the ultrafiltration through semipermeable tubular membranes. For small values of these parameters, perturbation analyses are carried out. From the analytical solutions of the perturbation problems, operating diagrams for a single hollow fiber are presented. It is shown that the ultrafiltration rate achieves a maximum as the volumetric flow rate of the perfusing blood is increased. The results in the present analysis demonstrate how that filtration maximum can be shifted to higher values by using a fiber material of greater hydraulic conductivity by using fibers of greater length/diameter ratio or by increasing the transmembrane pressure drop. The dimensionless treatment of the problem of ultrafiltration through hollow fibers makes it possible to use the same equations and conclusions presented in this work for other separation processes such as desalination.

DEVELOPMENT OF THE THEORETICAL MODEL

The artificial kidney, which is studied in the present work, is composed of a system of parallel hollow fibers, each fiber having a length L and an internal radius R. The fibers are surrounded by the filtrate which is enclosed within the main shell of the device, as shown in Figure 1. The hollow fibers receive blood through a manifold header connected to an artery of the patient having pressure p_1, protein concentration c_1, and hematocrit H_1. Blood leaves the fibers through another header with the pressure p_2, protein concentration c_2, and hematocrit H_2. The reason for the change of protein concentration and hematocrit is the loss of water due to the ultrafiltration into the surrounding diafiltrate. The following assumptions underly the theoretical model:

1. The walls of the hollow fibers are ideally selective membranes; that is, cellular particles and plasma protein are retained internally, whereas water and toxins can permeate freely.
2. The hydraulic conductivity K of the fiber walls, as defined in Equation (2), is constant over the entire fiber length L.
3. The hydrostatic pressure p_d of the external diafiltrate is constant.
4. The change in blood viscosity μ along the fibers due to increasing protein concentration and hematocrit is neglected.
5. The two phase character of blood, that is, flow of plasma and cellular particles, is neglected for the axial fluid transport.
6. Radial pressure and concentration gradients in the blood flow are neglected (usually denoted as hydraulic approach).
7. Diffusive axial transport of proteins in the blood is negligible compared with the convective transport.
8. The Reynolds number, based on the average linear velocity of the blood in the fibers, the internal fiber diameter, blood density, and viscosity, is usually less than 10. Therefore, hydraulic entrance effects at the beginning of the fibers can be neglected.
9. Steady flow.

Recently, Papenfuss and Gross (1977) studied the effect of axial variation of blood viscosity due to increasing protein concentration and hematocrit. Replacement of assumption 4 by this more general approach yielded no appreciable deviation from our numerical results for hollow fiber ultrafiltration in the present work. Therefore, our use of assumption 4 is justified.

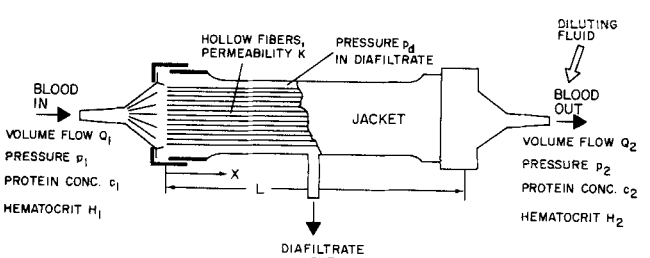

Fig. 1. Hollow-fiber artificial kidney.

The major contribution to the volume fraction for all cellular particles stems from the red cells (erythrocytes), whereas the volume fraction of all the other particles is negligibly small. In contrast to the axial blood flow, the presence of red cells must be taken into account when the transmembrane flow is determined. This is so because a substantial fraction of the blood, corresponding to the volume of the red cells in the fibers, does not participate in the transmembrane exchange.

Since all hollow fibers are the same, it is sufficient to consider only a single fiber in order to investigate the ultrafiltration in the device. The volume flow Q of the blood within a single fiber is the sum of the volume flow of the plasma and the erythrocytes

$$Q(x) = Q_{pl}(x) + Q_e \tag{1}$$

Following Katchalsky's approach of applying the principles of nonequilibrium thermodynamics to membrane transport results in an equation for the volumetric flux of the solvent of a dilute solution across a tubular membrane

$$J = \frac{1}{2\pi R}\frac{dQ_{pl}}{dx} = -K\cdot[p(x) - p_d - \pi_{pl}(x) + \pi_d] \tag{2}$$

(see Katchalsky and Curran, 1965; Middleman, 1972). In the present study, the solutes are the plasma proteins whereas the solvent itself is an aqueous solution of salts and toxins. Equation (2) is valid for an ideally selective membrane and is in the form of Starling's hypothesis (1896) which is used in physiology to study transcapillary fluid exchange. The colloid osmotic pressure in the filtrate π_d, which appears in Equation (2), is zero owing to assumption 1.

It is apparent from Equation (2) that the local effective ultrafiltration pressure is less than the local hydrostatic pressure difference across the fiber wall, $p(x) - p_d$. The value of the ultrafiltrate pressure is decreased by the local colloid osmotic pressure π_{pl} due to the presence of the plasma proteins which cannot penetrate the semipermeable fiber wall.

It should be emphasized that the colloid osmotic pressure must not be confused with the total osmotic pressure in the blood. The total osmotic pressure exceeds the colloid osmotic pressure by several orders of magnitude and results from the presence of salts in the blood. The plasma proteins provide a negligible contribution to the total osmotic pressure. When the red cells are exposed to changing total osmotic pressure, they experience a change in volume. Since the salt concentration in the blood remains constant in the hollow fibers, the red cell volume does not change, and Q_e in Equation (1)

is a constant. Thus, dQ_{pl}/dx in Equation (2) can be replaced by dQ/dx.

The colloid osmotic pressure increases as the concentration of the proteins increases. For small protein concentrations, the osmotic pressure can be expanded in a power series

$$\pi_{pl}(x) = \alpha c(x) + \beta c^2(x) + \delta c^3(x) \tag{3}$$

where α, β, and δ are empirical constants which have been determined by Landis and Pappenheimer (1963) for 37°C as $\alpha = 2.1$ mm Hg/(g/100 ml), $\beta = 0.16$ mm Hg/(g/100 ml)^2, and $\delta = 0.009$ mm Hg/(g/100 ml)^3.

Since the fiber wall is impermeable to the plasma proteins, the mass flow rate of the proteins must be constant:

$$c(x) \cdot Q_{pl}(x) = B \tag{4}$$

B is a constant that is determined from the initial conditions

$$B = c(0) \cdot Q_{pl}(0) = c_1(Q_1 - Q_e) \tag{5}$$

Using the definition of the hematocrit of the blood at the entrance of the system

$$H_1 = Q_e/Q_1 \tag{6}$$

and substituting into Equations (4) and (5), we obtain

$$c(x) = c_1 \frac{(1 - H_1)Q_1}{Q(x) - H_1 Q_1} \tag{7}$$

The local filtration rate is, in general, very small compared with the local axial volume flow of blood. Therefore, as a first approximation, we use the generalized Poiseuille relation between the axial pressure gradient and the local volume flow:

$$\frac{dp}{dx} = -\frac{8\mu}{\pi R^4} Q(x) \tag{8}$$

Thus, the ultrafiltration within the device is defined by two coupled differential Equations (2) and (8) together with Equations (3) and (7). The boundary conditions are

$$\left.\begin{aligned} x = 0:\ p(x) &= p_1 \\ x = L:\ p(x) &= p_2 \end{aligned}\right\} \tag{9}$$

The governing equations can be nondimensionalized by using the following dimensionless quantities:

$$\left.\begin{aligned} x^* &= \frac{x}{L} \quad \alpha^* = \frac{\alpha c_1}{p_1 - p_d} \quad P^* = \frac{p - p_d}{p_1 - p_d} \\ c^* &= \frac{c}{c_1} \quad \beta^* = \frac{\beta c_1^2}{p_1 - p_d} \\ Q^* &= \frac{Q}{Q_{ref}} \quad \delta^* = \frac{\delta c_1^3}{p_1 - p_d} \quad \pi^*_{pl} = \frac{\pi_{pl}}{p_1 - p_d} \end{aligned}\right\} \tag{10}$$

where Q_{ref} is the abbreviation for

$$Q_{ref} = R^2\pi \frac{(p_1 - p_d)R^2}{\mu L} \tag{11}$$

Substitution of Equation (10) into Equations (2), (3), (7), and (8) yields the following set of dimensionless equations:

$$\frac{dP^*}{dx^*} = -8Q^*(x^*) \tag{12}$$

$$\frac{dQ^*}{dx^*} = -2\frac{K\mu}{R}\left(\frac{L}{R}\right)^2 [P^*(x^*) - \pi^*_{pl}] \tag{13}$$

$$\pi^*_{pl} = \alpha^* c^*(x) + \beta^* c^{*2}(x^*) + \delta^* c^{*3}(x^*) \tag{14}$$

$$c^*(x^*) = \frac{Q^*_1[1 - H_1]}{Q^*(x^*) - H_1 Q^*_1} \tag{15}$$

The transformed boundary conditions are

$$\left.\begin{aligned} x^* = 0:\ P^* &= 1 \\ x^* = 1:\ P^* &= \frac{p_2 - p_d}{p_1 - p_d} = 1 - \sigma \end{aligned}\right\} \tag{16}$$

The change in the axial volume flow dQ^*/dx^* represents the local filtration rate. The total filtration rate Ψ of plasma into the diafiltrate is

$$\Psi = Q^*_1 - Q^*_2 = (1 - H_1) \cdot Q_1^*(1 - 1/c_2^*) \tag{17}$$

The factor in Equation (13)

$$\frac{K\mu}{R}\left(\frac{L}{R}\right)^2 = \epsilon \tag{18}$$

is a dimensionless parameter which plays a key role in characterizing the ultrafiltration in a hollow fiber. It is actually a combination of two dimensionless parameter $\kappa = K\mu/R$ and L/R, where κ has been used by Lew and Fung (1969) and Oka and Murata (1970) to analyze fluid exchange between blood and tissue. The present work, however, demonstrates that under the assumptions made herein, the ratio L/R does not occur explicitly in the equations but only in the combination shown in Equation (18) This important parameter ϵ is denoted as ultrafiltration parameter. A physical interpretation of the ultrafiltration parameter ϵ is apparent when Equation (18) is grouped in the following way:

$$\epsilon = \frac{1}{16} \cdot \frac{8\mu L/(\pi R^4)}{(2\pi RLK)^{-1}} \tag{19}$$

Excluding the numerical factor 1/16, ϵ is the ratio between the hydraulic resistance to axial flow in a tube of length L and the hydraulic resistance to transmembrane flow through a tubular membrane of the same length, see Equations (2) and (8).

Asymptotic Solution for Small Values of the Ultrafiltration Parameters

For small values of the parameter ϵ, the solutions of Equations (12) to (15) can be represented by the following asymptotic expansions (see Van Dyke, 1975):

$$P^* = p^{(1)} + \epsilon p^{(2)} + \epsilon^2 p^{(3)} + \dots \tag{20}$$

$$Q^* = Q^{(1)} + \epsilon Q^{(2)} + \epsilon^2 Q^{(3)} + \dots \tag{21}$$

$$\Psi = \Psi^{(1)} + \epsilon \Psi^{(2)} + \epsilon^2 \Psi^{(3)} + \dots \tag{22}$$

first order second order third order

We introduce these expansions in the equations for axial and transmural fluid transport (12) to (14), where the protein concentration has been replaced by Equation (15). Collection of terms of the same order of magnitude, that is, $0(1)$, $0(\epsilon)$, $0(\epsilon^2)$, . . ., yields equations for the first-order terms, second-order terms, third-order terms, etc. The equations for the first-order terms $0(1)$ are

$$\frac{dQ^{(1)}}{dx^*} = 0 \tag{23}$$

$$\frac{dp^{(1)}}{dx^*} = -8Q^{(1)} \tag{24}$$

with the boundary conditions

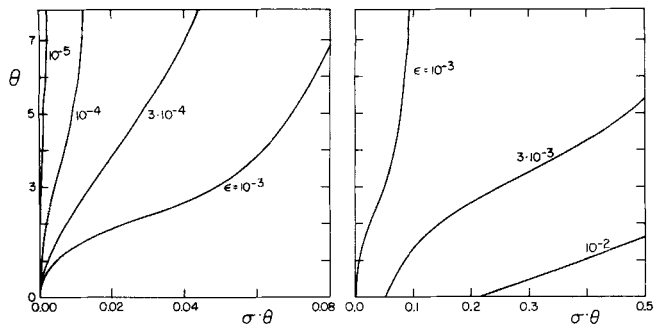

Fig. 2. Valid and invalid regions for asymptotic expansion for $\epsilon \to 0$.

$$x^* = 0: \; p^{(1)} = 1 \tag{25}$$

$$x^* = 1: \; p^{(1)} = 1 - \sigma \tag{26}$$

The solutions to the first-order equations are

$$p^{(1)} = 1 - \sigma x^* \tag{27}$$

$$Q^{(1)} = \sigma/8 = \text{const} \tag{28}$$

$$\Psi^{(1)} = 0 \tag{29}$$

It should be noted that $c^*(x^*) = 1$ for $\epsilon = 0$. The concentration does not change along the length of the fiber, since no filtration takes place. The equations then reduce to the classical Poiseuille equation for flow through impermeable tubes.

The equations for the second-order terms $0(\epsilon)$ are

$$\frac{dQ^{(2)}}{dx^*} = -2[p^{(1)} - (\alpha^* + \beta^* + \delta^*)] \tag{30}$$

$$\frac{dp^{(2)}}{dx^*} = -8Q^{(2)} \tag{31}$$

with the boundary conditions

$$\left.\begin{aligned} x^* = 0: \; p^{(2)} = 0 \\ x^* = 1: \; p^{(2)} = 0 \end{aligned}\right\} \tag{32}$$

The solutions to the second-order equations are

$$p^{(2)} = -\frac{8\sigma}{3}(x^{*3} - x^*) + 8G(x^{*2} - x^*) \tag{33}$$

$$Q^{(2)} = \sigma(x^{*2} - 1/3) - 2G(x^* - 1/2) \tag{34}$$

$$\Psi^{(2)} = 2G - \sigma \tag{35}$$

where the following abbreviation was used:

$$G = 1 - (\alpha^* + \beta^* + \delta^*) \tag{36}$$

The equations for the third-order terms $O(\epsilon^2)$ are

$$\frac{dQ^{(3)}}{dx^*} = \frac{16\sigma}{3}(x^{*3} - x^*) - 16G(x^{*2} - x^*) - 16\frac{M}{\sigma}(\sigma x^{*2} - 2Gx^*) \tag{37}$$

$$\frac{dp^{(3)}}{dx^*} = -8Q^{(3)} \tag{38}$$

with the boundary conditions

$$\left.\begin{aligned} x^* = 0: \; p^{(3)} = 0 \\ x^* = 1: \; p^{(3)} = 0 \end{aligned}\right\} \tag{39}$$

In Equation (37), M is the abbreviation for

$$M = \frac{\alpha^* + 2\beta^* + 3\delta^*}{1 - H_1} \tag{40}$$

The solutions to the third-order equations are

$$p^{(3)} = 256\left\{\frac{G}{2}\left(\frac{x^{*4}}{12} - \frac{x^{*3}}{6} + \frac{x^*}{12}\right) - \frac{\sigma}{6}\left(\frac{x^{*5}}{20} - \frac{x^{*3}}{6} + \frac{7x^*}{60}\right) - \frac{M}{\sigma}\left[G\left(\frac{x^{*3}}{6} - \frac{x^*}{6}\right) - \frac{\sigma}{6}\left(\frac{x^{*4}}{4} - \frac{x^*}{4}\right)\right]\right\} \tag{41}$$

$$Q^{(3)} = -32\left\{\frac{G}{2}\left(\frac{x^{*3}}{3} - \frac{x^{*2}}{2} + \frac{1}{12}\right) - \frac{\sigma}{6}\left(\frac{x^{*4}}{4} - \frac{x^{*2}}{2} + \frac{7}{60}\right) - \frac{M}{\sigma}\left[G\left(\frac{x^{*2}}{2} - 1/6\right) - \frac{\sigma}{6}(x^{*3} - 1/4)\right]\right\} \tag{42}$$

$$\Psi^{(3)} = 16\left\{\frac{\sigma}{12} + \frac{2M - G}{6} - \frac{GM}{\sigma}\right\} \tag{43}$$

Using Equation (21), the local protein concentration $c^*(x^*)$ can be calculated from Equation (15).

The numerical evaluation of the previous solutions obtained by the perturbation analysis requires a set of numbers for α^*, β^*, and δ^*. These numbers can be obtained by specifying c_1 and $p_1 - p_d$ according to Equation (10). We express the pressure difference $p_1 - p_d$ as multiples of 100 mmHg and define

$$\theta = \frac{p_1 - p_d}{100 \text{ mmHg}} \tag{44}$$

The asymptotic expansions (20) to (22) do not hold for very small values of σ. It can be seen in Equations (41) to (43) that σ appears in the denominator, so that the asymptotic solution breaks down for $\sigma \to 0$. The reason is that the differential Equations (12) to (15) lead to very steep gradients of the protein concentration at the entrance of the hollow fiber when σ tends to zero. This gives rise to a singular perturbation problem which will be discussed further below. Those values of σ for which the asymptotic solution for $\epsilon \to 0$ should not be used are shown in Figure 2. These critical values of σ have been determined from a comparison of the asymptotic solutions, both with numerical solutions of the full set of differential equations using very small step sizes and with the solution of the singular perturbation problem for $\sigma \to 0$. The curves shown in Figure 2 divide the field into regions in which the asymptotic solutions given above are valid and invalid. An example may serve to demonstrate this. Consider the curve for $\epsilon = 10^{-3}$. The point ($\sigma \cdot \theta = 0.03$, $\theta = 2$) is located in the region where the asymptotic solution may be used, whereas the combination ($\sigma \cdot \theta = 0.02$, $\theta = 2$) is located in the region where the asymptotic solution breaks down. Figure 2 shows that the region of validity for the asymptotic expansion shrinks rapidly when ϵ becomes greater than about 10^{-3}. When $\epsilon > 10^{-2}$, the region of validity is reduced to a very small area. In this case, we recommend that the full set of differential equations, Equations (12) to (15), be solved numerically.

Asymptotic Solution for Small Values of the Dimensionless Axial Pressure Drop σ

The boundary conditions (16) suggest the transformation

$$P^* = 1 - \sigma\hat{P}(x^*) \tag{45}$$

TABLE 1. PROTEIN CONCENTRATION OF FIRST-ORDER OUTER SOLUTION

θ	0	1	2	3	4	5	6	7	8	9
$\frac{\tilde{c}^{(1)} \cdot c_1}{\text{g/100 ml}}$	0.0000	15.1627	21.0959	25.2532	28.5558	31.3397	33.7701	35.9408	37.9120	39.7229

Combining Equation (12) with (13) and Equation (12) with (15), we obtain

$$\sigma\hat{P}'' + 16\epsilon[1 - \sigma\hat{P} - (\alpha^* c^* + \beta^* c^{*2} + \delta^* c^{*3})] = 0 \tag{46}$$

$$c^* = \frac{(1 - H_1)\hat{P}'(0)}{\hat{P}'(x^*) - H_1\hat{P}'(0)} \cdot c^*(0) \tag{47}$$

and the boundary conditions

$$\hat{P}(0) = 0, \quad \hat{P}(1) = 1 \tag{48}$$

Primes denote differentiation with respect to x^*. Since the protein concentration at the entrance of the fiber must be equal to that of the entering blood, that is, $c(0) = c_1$, it is clear that $c^*(0)$ must be one. However, when the axial pressure drop σ approaches zero, Equation (46) cannot satisfy this condition. This is a singular perturbation problem which can be treated using the method of matched asymptotic expansions, see Van Dyke (1975). The singularity appears at the fiber entrance where the concentration gradient becomes very large. The strategy is to determine asymptotic solutions with respect to the perturbation parameter σ in a region of the fiber which excludes the singularity (that is, the outer solution) and in a region which contains the singularity (that is, the inner solution), and to match these solutions properly.

Introducing the outer expansion

$$\hat{P}(x^*) = f^{(1)}(x^*) + \sigma f^{(2)}(x^*) + \sigma^2 f^{(3)}(x^*) + \dots \tag{49}$$

$$c(x^*) = \tilde{c}^{(1)}(x^*) + \sigma\tilde{c}^{(2)}(x^*) + \sigma^2\tilde{c}^{(3)}(x^*) + \dots \tag{50}$$

into Equation (46) and collecting terms of order $0(1)$, we get a cubic equation for $\tilde{c}^{(1)}$:

$$\alpha^*\tilde{c}^{(1)} + \beta^*[\tilde{c}^{(1)}]^2 + \delta^*[\tilde{c}^{(1)}]^3 - 1 = 0 \tag{51}$$

For $\theta = 0 \dots 9$, the values for the product $\tilde{c}^{(1)} \cdot c_1$ are listed in Table 1. These values are independent of x^*, the initial concentration c_1, the hematocrit H_1, and the ultrafiltration parameter ϵ (as long as $\epsilon > 0$). From Equation (12), we obtain by integration

$$f^{(1)}(x^*) = 8A(x^* - 1) + 1 \tag{52}$$

where the constant A will be determined from matching the outer and inner expansions.

For the inner expansion, which is valid near the fiber entrance, a stretched inner variable

$$z = \frac{x^*}{\sigma} \tag{53}$$

must be introduced. The inner expansion is then given by

$$\hat{P}(z, \sigma) = \sigma F^{(1)}(z) + \sigma^2 F^{(2)}(z) + \sigma^3 F^{(3)}(z) + \dots \tag{54}$$

$$c^*(z, \sigma) = C^{(1)}(z) + \sigma C^{(2)}(z) + \sigma^2 C^{(3)}(z) + \dots \tag{55}$$

The inner expansion is introduced into Equations (46) and (47) and terms of order $0(1)$ are compared, yielding equations for $\ddot{F}^{(1)}$ and $C^{(1)}$:

$$\ddot{F}^{(1)} + 16\epsilon\{1 - [\alpha^* C^{(1)} + \beta^* C^{(1)^2} + \delta^* C^{(1)^3}]\} = 0 \tag{56}$$

$$C^{(1)} = \frac{(1 - H_1)\dot{F}^{(1)}(0)}{\dot{F}^{(1)} - H_1\dot{F}^{(1)}(0)} \tag{57}$$

The boundary condition at the fiber entrance is

$$F^{(1)}(0) = 0 \tag{58}$$

Using the matching condition that for large values of z, when $z \to \infty$, the inner concentration $C^{(1)}$ approaches the outer concentration $\tilde{C}^{(1)}$, we obtain the second boundary conditions:

$$\dot{F}^{(1)}(z \to \infty) = \dot{F}^{(1)}(0) \cdot \left[\frac{1 - H_1}{\tilde{c}^{(1)}} + H_1\right] \tag{59}$$

Matching outer and inner pressures yields

$$\left.\begin{aligned} A &= \frac{1}{8} \\ \dot{F}^{(1)}(0) &= \left[\frac{1 - H_1}{\tilde{c}^{(1)}} + H_1\right]^{-1} \end{aligned}\right\} \tag{60}$$

Thus, the analytical solution for the first-order outer flow is

$$f^{(1)}(x^*) = x^* \tag{61}$$

which means that in the limiting case $\sigma \to 0$, the flow in the fiber is a Poiseuille flow. The solution for the inner flow must be determined numerically from Equation (56) and (57) using the boundary conditions (58) to (60).

The volume flow which enters the fiber and the filtration rate can be found directly:

$$\left.\begin{aligned} Q_1^* &= -\frac{\sigma}{8}\dot{F}^{(1)}(0) + 0(\sigma^2) \\ \Psi &= -\frac{\sigma}{8}[\dot{F}^{(1)}(0) + 1] + 0(\sigma^2) \end{aligned}\right\} \tag{62}$$

From Equation (62), we obtain

$$\Psi = Q_1^*\left[1 + \frac{1}{\dot{F}^{(1)}(0)}\right] + 0(\sigma)$$

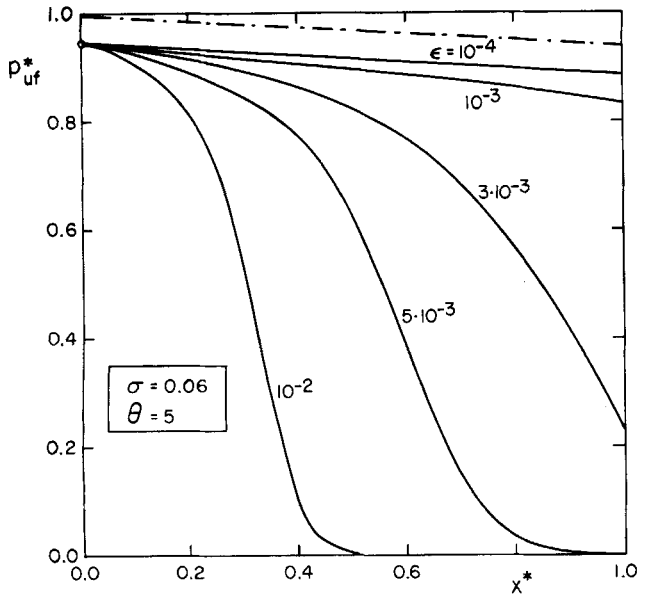

Fig. 3. Development of net ultrafiltration pressure along fiber axis for different values of the ultrafiltration parameter.

$$= Q_1^*(1 - H_1)(1 - 1/c^{(1)}) + 0(\sigma) \quad (63)$$

This equation can also be derived from Equation (17). Another useful result is the second-order outer solution for the protein concentration. From Equations (46) and (61), it follows that

$$\tilde{c}^{(2)} = \frac{-x^*}{\alpha^* + 2\beta^*\tilde{c}^{(1)} + 3\delta^*[\tilde{c}^{(1)}]^2} \quad (64)$$

It is noteworthy that these asymptotic results are independent of the ultrafiltration parameter ϵ. In contrast to the outer solution, the inner solution depends on the hematocrit.

RESULTS AND DISCUSSION

The equations resulting from the perturbation analysis for $\epsilon \to 0$ have been evaluated for the case of human blood; that is, $H_1 = 0.4$ and $c_1 = 7$ g/100 ml. The range

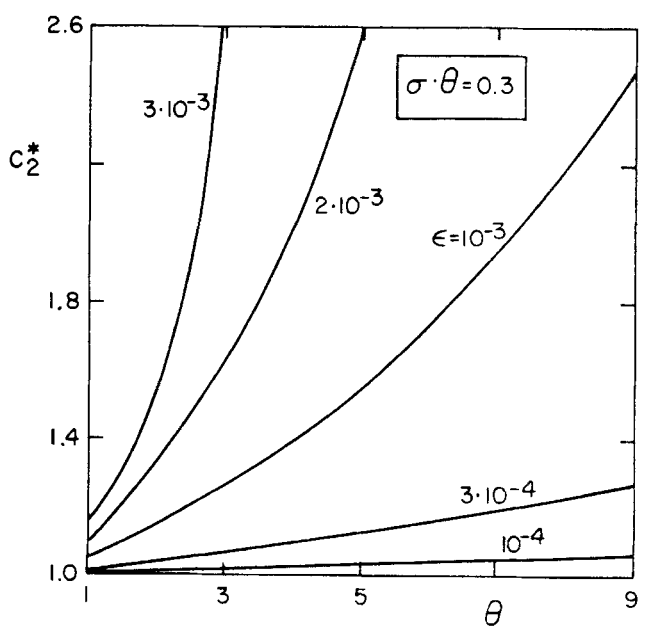

Fig. 5. Protein concentration at discharge end of fiber as a function of transmembrane pressure drop and ultrafiltration parameter.

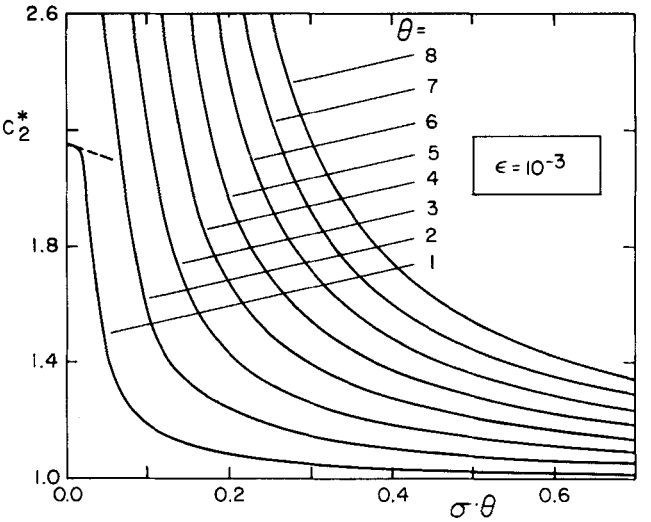

Fig. 4. Protein concentration at discharge end of fiber as a function of axial and transmembrane pressure drop.

for the ultrafiltration parameter was chosen to be $10^{-4} \leq \epsilon \leq 10^{-2}$. This range covers the values for hollow fibers which are now marketed commercially for use in artificial kidney machines. The dimensionless transmembrane pressure drop θ was varied between 1 and 8. This is the range of application in laboratory studies of blood ultrafiltration. The dimensionless axial pressure drop, which essentially determines the axial blood volume flow, was expressed by σ or, alternatively, by the product $\sigma\theta$:

$$\sigma\theta = \frac{p_1 - p_2}{100 \text{ mmHg}} \quad (65)$$

$\sigma\theta$ was varied between 0 and 0.7. For those values of σ, for which the asymptotic expansion for $\epsilon \to 0$ was no longer valid (see Figure 2), we solved Equations (12) to (16) numerically using the Runge-Kutta method. For very small values of σ, we used the equations which resulted from the perturbation analysis of $\sigma \to 0$.

Space limitations permit the presentation of only selected results which are discussed in Figures 3 to 9. Figure 3 shows the net ultrafiltration pressure

$$p_{uf}^* = p^* - \pi_{pl}^* \quad (66)$$

as a function of the axial position x^* for various values of the ultrafiltration parameter ϵ and for $\theta = 5$ and $\sigma\theta = 0.3$. The net ultrafiltration pressure is directly proportional to the local permeation velocity. The following results are apparent from this figure:

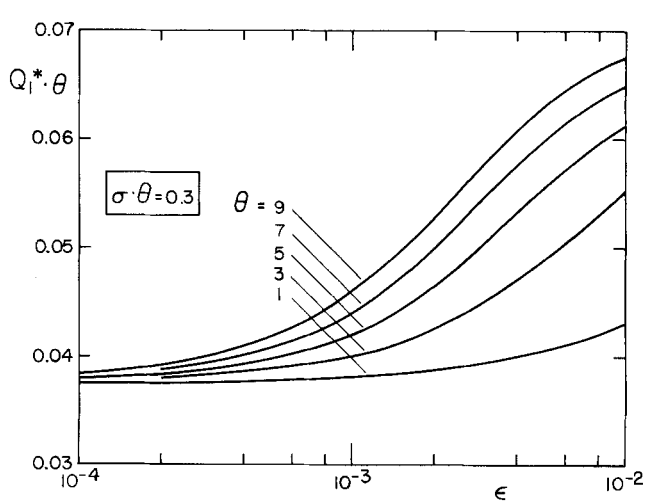

Fig. 6. Initial blood volume flow as a function of ultrafiltration parameter and transmembrane pressure drop.

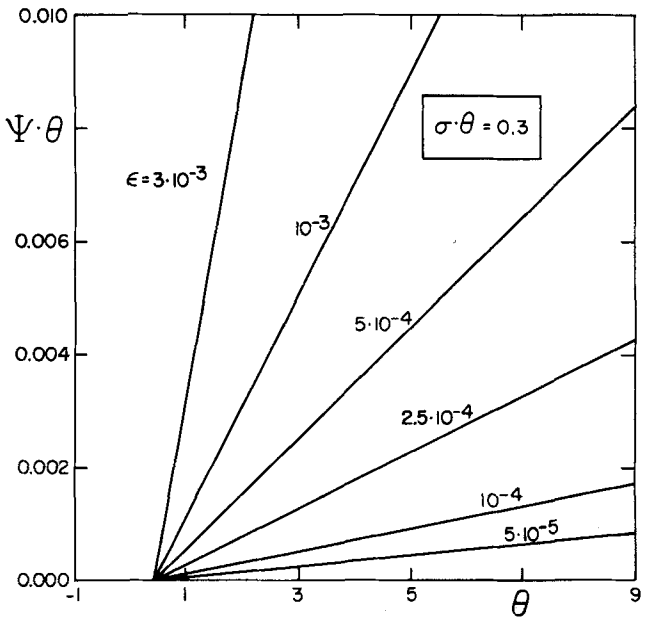

Fig. 7. Filtration rate as a function of transmembrane pressure drop and ultrafiltration parameter.

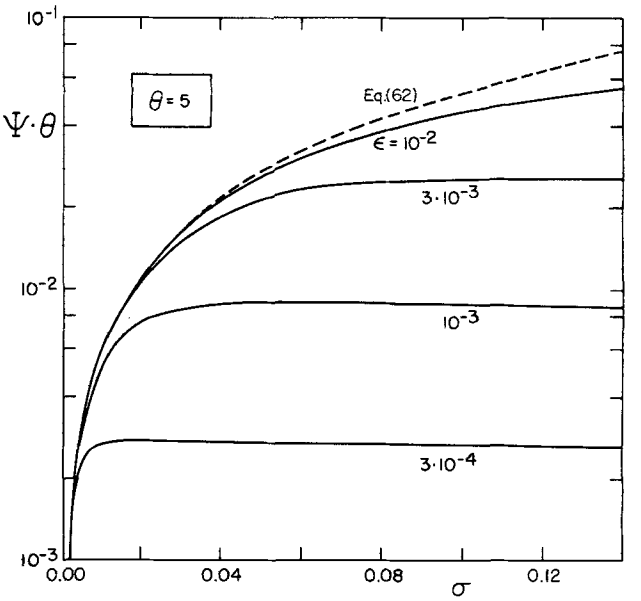

Fig. 8. Filtration rate as a function of axial pressure drop and ultrafiltration parameter.

1. The permeation velocity is not constant along the fiber axis.
2. When the ultrafiltration parameter is small, the permeation velocity decreases linearly with the axial distance from the entrance of the fiber.
3. When the ultrafiltration parameter ϵ is increased, for example by choosing a fiber material of greater hydraulic conductivity, the axial reduction of the permeation velocity increases. The permeation velocity is then a strongly nonlinear function of x^* and may tend to zero or even to negative values (= reabsorption) before the end of the fiber is reached.

This behavior can be explained by the increase in the protein concentration along the fiber axis due to fluid loss causing a concomitant increase in the colloid osmotic pressure. The colloid osmotic pressure is the difference between the dash-dotted line and the solid lines in Figure 3, where the dash-dotted line represents the hydrostatic pressure drop across the wall; this pressure drop differs only slightly for the selected values of ϵ. When $\epsilon = 10^{-2}$, only the first half of the fiber behaves as an active ultrafilter, whereas the second half becomes effectively impermeable since the increased colloid osmotic pressure balances the transmembrane hydrostatic pressure drop. The latter is frequently denoted as filtration equilibrium. It should be emphasized that this limitation of a hollow fiber for ultrafiltration has nothing to do with concentration polarization which we do not consider in the present work. Further, it can be concluded from Figure 3 that an analytical approach to hollow fiber ultrafiltration, using the assumption of constant permeation velocity (Sherwood et al., 1965), must lead to questionable results.

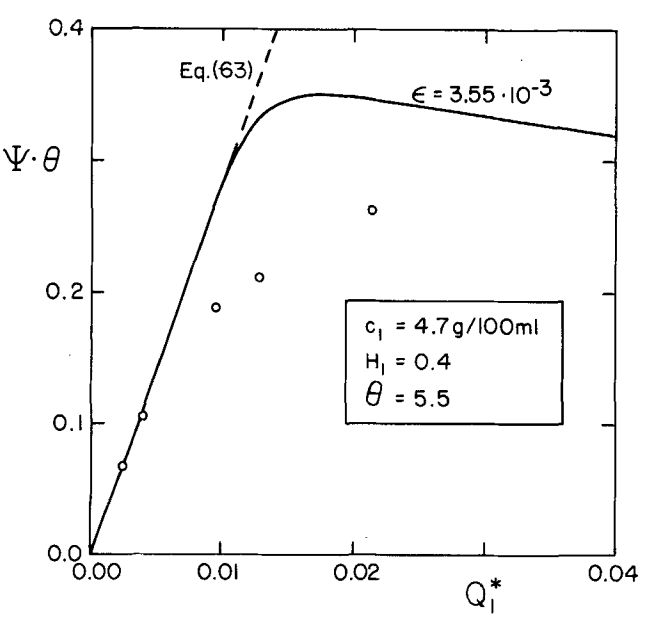

Fig. 9. Filtration rate as a function of initial blood volume flow. Experimental results from Colton et al. (1975).

The variation of the protein concentration with the parameters σ, θ, and ϵ is discussed in Figures 4 and 5, where the values of the concentration at the discharge end of the fiber are shown. From our analysis and the previous discussion, it is clear that the protein concentration c_2^* increases when ϵ or θ increase. The same is true when σ decreases because the mean transmembrane hydrostatic pressure drop, averaged over the entire fiber length, then attains higher values. The value at $\sigma = 0$, which could be shown only for $\theta = 1$, is from Table 1. The dotted line in Figure 4 is the tangent at $\sigma = 0$ and is from Equation (64).

For $\epsilon = 0$, that is, the impermeable tube, the initial blood volume flow at the entrance of the fiber is proportional to the axial pressure drop σ according to Poiseuille's law, Equation (28). As ϵ is increased, however, the σ remains constant, the initial blood volume flow also increases. This result is shown in Figure 6. The increase in the initial blood flow becomes more significant when the transmembrane pressure drop is enlarged. This is so because the underpressure in the surrounding filtrate acts as a suction force on the blood.

The previous discussion serves as background for the interpretation of the behavior of the filtration rate under various conditions, which are shown in Figures 7 through 9. We used the product $\Psi \cdot \theta$

$$\Psi \cdot \theta = \frac{\mu \cdot L}{R^4 \pi \cdot 100 \text{ mmHg}} \cdot (Q_1 - Q_2) \qquad (67)$$

instead of Ψ to characterize the dimensionless filtration rate. For simplicity, this product will also be denoted as filtration rate. Figure 7 shows the following:

1. The filtration rate increases linearly with the transmembrane pressure drop.

2. A positive threshold value of the transmembrane pressure drop θ is necessary to overcome the colloid osmotic pressure in the fiber and, consequently, to achieve filtration. In our example, this value is about 0.5. The dependence of the threshold value on the membrane characteristics is very weak.

3. The degree of the increase in the filtration rate depends on the ultrafiltration parameter ϵ. When ϵ becomes greater, the filtration rate increases more rapidly with increasing θ.

Our findings under 1 and 2 are supported by several experimental investigations on hollow fiber ultrafiltration (see, for example, Maeda et al., 1974). In the same work, our statement given under 3 is also confirmed by experiments. However, statement 3 should be restricted to values of σ which are not too close to zero, since the filtration rate becomes independent of ϵ as $\sigma \to 0$. This is shown in Figure 8. The dashed line is the result of the singular perturbation problem which arises when σ approaches zero. It is important to note that for the given set of parameters θ, H_1, and c_1, all solutions of the differential Equations (12) to (16) must fall beneath the dashed line. Thus, the asymptotic result for $\sigma \to 0$ separates valid from invalid solutions.

Figure 8 shows that with increasing axial pressure drop, the filtration rate increases until a maximum is achieved. The maximum value depends on the ultrafiltration parameter ϵ. Further increase in the axial pressure drop ϵ leads to a slight decrease in the filtration rate. The explanation for the occurrence of a filtration maximum has nothing to do with concentration polarization. It is a consequence of the interaction between the increase in colloid osmotic pressure due to filtration and the transmembrane hydrostatic pressure drop. The mean value of the latter averaged over the entire fiber length becomes smaller when σ in increased.

The occurrence of a filtration maximum is also apparent in Figure 9, where the filtration rate is plotted vs. the initial blood volume flow. The calculations were based on data for blood and hollow fiber characteristics which were reported by Colton et al. (1975). From their extensive studies of blood ultrafiltration, we chose that data which were determined with bundles of 200 hollow fibers with internal diameters varying between 213 and 234 μm. The active fiber lengths varied between 17 and 18.4 cm, and the hydraulic conductivity K was $4.364 \cdot 10^{-5}$ cm/(min·mm Hg). The transmembrane pressure drop was 550 mm Hg. We restrict ourselves to a typical example with $2R = 220$ μm, $L = 17$ cm, $H_1 = 0.4$, and $c_1 = 4.7$ g/100 ml. For small values of Q_1^*, the filtration rate increases linearly with increasing Q_1^*, which confirms our asymptotic result, given in Equation (63). In this case, the first-order outer protein concentration $c^{(1)}$ is equal to 6.9345. When Q_1^* exceeds the value 0.005, an increasing deviation between the theoretical and experimental results appears. This demonstrates the detrimental effects of reduction of the effective hydraulic conductivity due to clogged pores and concentration polarization. No efforts were undertaken in the work of Colton et al. to avoid these effects. However, when Q_1^* increases further, the deviation between the theoretical and experimental results becomes smaller. The explanation for this is that the enlarged wall shear stress removes protein molecules in increasing amounts from the plugged pores and, thus, tends to restore the original hydraulic permeability.

ACKNOWLEDGMENT

This research was supported by Grant Pa 216/2 of the Deutsche Forschungsgemeinschaft e.V.

NOTATION

A = constant in Equation (52)
B = constant, defined in Equation (5)
c = plasma protein concentration
C = function used for inner expansion of protein concentration, Equation (55)
$\tilde{c}$ = function used for outer expansion of protein concentration, Equation (50)
f = function used for outer expansion of pressure, Equation (49)
F = function used for inner expansion of pressure, Equation (54)
G = abbreviation, defined in Equation (36)
H = hydraulic conductivity of fiber wall
j = volumetric flux of solvent across membrane
K = hydraulic permeability of fiber wall
L = fiber length
M = abbreviation, defined in Equation (40)
p = hydrostatic pressure
$\hat{P}$ = transformed hydrostatic pressure, Equation (45)
Q = volumetric flow rate
R = internal radius of fiber
x = axial coordinate along the fiber
z = x^*/σ, inner coordinate

Greek Letters

α = constant in Equation (3)
β = constant in Equation (3)
δ = constant in Equation (3)
ϵ = ultrafiltration parameter, Equation (18)
κ = $K\mu/R$, dimensionless parameter
π = colloid osmotic pressure
Ψ = total filtration rate
σ = dimensionless pressure drop, Equation (16)
θ = dimensionless transmembrane pressure drop, Equation (44)
μ = blood viscosity

Superscripts

* = dimensionless quantity
$^{(1)}$ = first-order term of asymptotic expansion
$^{(2)}$ = second-order term of asymptotic expansion
$^{(3)}$ = third-order term of asymptotic expansion

Subscripts

d = diafiltrate
e = erythrocyte, red blood cell
pl = blood plasma
ref = reference value
uf = ultrafiltration
1 = fiber inlet
2 = fiber outlet

LITERATURE CITED

Charm, S. E., and G. S. Kurland, *Blood Flow and Microcirculation*, John Wiley, New York (1974).

Colton, C. K., L. W. Henderson, C. A. Ford, and M. J. Lysaght, "Kinetics of Hemodiafiltration. I. In vitro Transport Characteristics of a Hollow-Fiber Blood Ultrafilter," *J. Lab. Clin. Med.*, 85, 355 (1975).

Cooney, D. O., "Biomedical Engineering Principles: An Introduction to Fluid, Heat, and Mass Transport Processes," in *"Biomedical Engineering and Instrumentation Series*, G. A. Bekey and D. D. Reneau, eds., Vol. 2, Marcel Dekker, New York (1976).

Gill, W. N., L. J. Derzansky, and M. R. Doshi, "Convective Diffusion in Laminar and Turbulent Hyperfiltration (Reverse Osmosis) Systems," in *Surface and Colloid Science*, E. Matijevic, ed., Vol. 4, Wiley, New York (1971).

Gill, W. N., and B. Bansal, "Hollow Fiber Reverse Osmosic

Systems, Analysis and Design," *AIChE J.*, **19**, 823 (1973).
Huss, R. E., D. J. Marsh, and R. E. Kalaba, "Two Models of Glomerular Filtration Rate and Renal Blood Flow in the Rat," *Annals Biomed. Eng.*, 3, 72 (1975).
Katchalsky, A., and P. F. Curran, *Nonequilibrium Thermodynamics in Biophysics*, Harvard University Press, Cambridge, Mass. (1965).
Landis, E. M., and J. R. Pappenheimer, "Exchange of Substances Through the Capillary Walls," in *Handbook of Physiology*, Section 2: Circulation, Vol. 2, Chapt. 29, American Physiological Society, Washington, D.C. (1963).
Lew, H. S., and Y. C. Fung, "Flow in an Occluded Cylindrical Tube with Permeable Wall," *Zeit. Angew. Math. Phys.*, **20**, 750 (1969).
Maeda, K., A. Saito, T. Shimoji, I. Amano, T. Manji, S. Kawaguchi, K. Kobayashi, Y. Fujisaki, and S. Eiga, "ASAHI Hollow Fiber Kidney (ASAHI HFK)—Progress Report," *Trans. Am. Soc. Artif. Int. Organs*, **20**, 344 (1974).
Middleman, S., *Transport Phenomena in the Cardiovascular System*, Wiley, New York (1972).
Oka, S., and T. Murata, "A Theoretical Study of the Flow of Blood in a Capillary with Permeable Wall," *Jap. J. Appl. Phys.*, **9**, 345 (1970).
Papenfuss, H. D., J. F. Gross, and F. Sanchez-Ruiz, "Application of Boundary-Layer Theory to Ultrafiltration Through Flat Semipermeable Membranes," Vol. 74, No. 172, 218 (1978).
Papenfuss, H. D., and J. F. Gross, "The Interaction Between Transmural Fluid Exchange and Blood Viscosity in Narrow Blood Vessels," *Biorheology*, **14**, 217 (1977).
Proceedings of the Tenth Annual Contractors' Conference of the Artificial Kidney Program of the National Institute of Arthritis, Metabolism, and Digestive Diseases, *DHEW Publication No. (NIH) 77-1442* (1977).
Sherwood, T. K., P. L. T. Brian, R. E. Fischer, and L. Dresner, "Salt Concentration at Phase Boundaries in Desalination by Reverse Osmosis," *Ind. Eng. Chem. Fundamentals*, **4**, No. 2, 113 (1965).
Starling, E. H., "On the Absorption of Fluid from the Connective Tissue Spaces," *J. Physiol.*, **19**, 312 (1896).
Van Dyke, M., *Perturbation Methods in Fluid Mechanics*, The Parabolic Press, Stanford, Calif. (1975).

Manuscript received February 17, 1977; revision received August 2, and accepted September 14, 1978.

R & D NOTES

Modified Yerzaunis, Plowright, and Smola Equilibrium Still

WEBSTER B. KAY

Department of Chemical Engineering
Ohio State University
Columbus, Ohio 43210

Yerazunis et al. (1964) have described an apparatus for the experimental determination of *V-L* equilibrium datum which, in its design, approaches very closely to what may be considered as the ideal equilibrium still. The still differs from others that have been described by Hala et al. (1958) in the very positive manner in which the liquid and vapor phases are brought together under constant temperature and pressure to insure that the composition of the coexisting phases represent the true equilibrium condition. In a research program, which involves the determination of the *V-L* equilibrium properties of liquid mixtures at low pressure, an equilibrium still has been constructed for use which is similar to the Yerazunis still in the design of the equilibrium section but differs in the location of the thermocouple for measuring the equilibrium temperature and in the method for withdrawing the samples from the still. Also, a separate insulating cap was constructed to fit over the equilibrium chamber to reduce the heat loss. These changes not only improve the design but greatly simplify the operation of the still.

The equilibrium cell was redesigned so that the thermocouple for measuring the equilibrium temperature is located in a well, imbedded in the equilibrium chamber, in order to insure a more precise measurement of the temperature. Next, the stopcock assembly was replaced by ports with rubber septums* through which samples of the equilibrium vapor condensate and the liquid could be withdrawn for analysis with a hypodermic syringe.

* Available only from Ace Glass, Inc., Vineland, New Jersey.